

RESEARCH

Open Access



Mechanical Response of Barricade to Coupled THMC Behavior of Cemented Paste Backfill

Di Wu^{*}, Wentao Hou, Shuai Liu and Huaibin Liu

Abstract

Cemented paste backfill (CPB), which is prepared by mixing tailings, binder and water, is widely used in underground mines for waste management and ground control. Since the CPB is delivered into mined-out areas in the form of fluid, a barricade needs to be constructed for retaining it during the process of its filling and hardening. Therefore, the barricade should have enough mechanical stability to ensure the safety of the backfill operation. The behavior of CPB, which is influenced by the thermal, hydraulic, mechanical and chemical (THMC) coupled processes, acts on the barricade and thus affects its mechanical response. In the present study, a numerical model is developed to predict and analyze the barricade mechanical performance in response to the coupled THMC behavior of CPB. The validity of the proposed model is then verified against two field case studies. Acceptable agreement between the model prediction results and in situ monitoring data proves the capability of the developed model in simulating the barricade pressure and displacement. Then, the validated model is used to investigate the effect of filling strategy on the barricade displacement. The obtained results can contribute to a better understanding of the barricade performance under various backfill conditions.

Keywords: cemented paste backfill, barricade, mechanical response, numerical model, stope

1 Introduction

Recently, cemented paste backfill (CPB) technology has become one of the most important and innovative technologies for sustainable mining and green mining. CPB is a heterogeneous material composed by tailings (normally account for a mass concentration between 70 and 85%), binder and water (Pokharel and Fall 2013). This technology is being widely and intensively employed in numerous underground mines all over the world, due to its irreplaceable safe, economic and environmental benefits for the mining industry, such as ground support, improvement of ore production, and mine waste management (Kesimal et al. 2003; Fall et al. 2005, 2008;

Ercikdi et al. 2009; Fall and Pokharel 2010; Mahlaba et al. 2011).

Freshly prepared CPB materials are placed into underground open stopes, and backfill barricades are built in each of the access ways into the stopes prior to stope filling, for retaining the fresh CPB slurries (Fall and Pokharel 2010). The crucial function of the barricade is to keep the fresh CPB in place to form the hardened CPB structure, which can thereby provide support for adjacent ore bodies and surrounding rocks. Therefore, the barricade is required to possess enough strength and stability to retain the CPB. Mining workers and engineers are greatly concerned about the barricade stability, especially during the inrush of the fresh CPB, which imposes lateral pressure on the barricade, and the pressure increases with the continuous filling of the CPB. In order to prevent the possible failure of the barricade induced by the excessive lateral pressure, an initial pouring is performed

*Correspondence: ustb_wudil@hotmail.com
School of Energy and Mining Engineering, China University of Mining and Technology-Beijing, Ding 11 Xueyuan Road, Haidian District, Beijing 100083, China
Journal information: ISSN 1976-0485 / eISSN 2234-1315

to form a plug, which is cured for a day or more and followed by a final filling (Thompson et al. 2009). However, this backfilling strategy delays the mining production. The insufficient strength of the barricade leads to its failure, but excessive strength of the barricade results in the increased mining operation costs. Hence, it is significant to design a suitable strength for the barricade to satisfy both the mechanical and economic requirements.

The lateral pressure of the placed CPB on the barricade varies with the consolidation of the CPB, which is controlled by complex thermal, hydraulic, mechanical and chemical (THMC) processes that occur in the CPB (Doherty 2015). Hydration of binder is a chemical reaction and generates hydration products, contributing to the consolidation of the CPB. With the hardening of the CPB, its lateral pressure on the barricade gradually stops to grow. The binder hydration process is exothermic and can thereby release heat to cause the development of thermal stress in the CPB. The process of binder hydration also consumes water, resulting in the evolution of pore water pressure and thus variation of effective stress in the CPB. Therefore, the mechanical response of the barricade to the coupled THMC behavior of the CPB should be assessed and discussed.

In-situ measurement is a direct and effective approach to investigate the evolution of the barricade pressure. In doing so, Belem et al. (2004) carried out a field measurement to indicate the evolution of the barricade pressure with the consolidation process of paste backfill at a gold mine. Yumlu and Guresci (2007) used a field monitoring program to investigate the pressure of paste backfill on the bulkhead at Inmet's Cayeli Mine. Thompson et al. (2009, 2012) installed total earth pressure cells (TEPCs) within the CPB and also on the barricade to investigate their pressure evolutions. Their studies can contribute to a better understanding of the correlation between the backfill pressure and barricade pressure. Similar field monitoring programs and methods were conducted by Helinski et al. (2011) and Doherty et al. (2015). Although in situ measurements can directly indicate the varying patterns in the barricade pressure and thus provide better understanding of the barricade behavior responding to the CPB placement and consolidation. Nevertheless, field tests affect normal production and increase operating costs.

In comparison with in situ measurements, numerical modeling and simulation are more favorable in some aspects, such as low operational cost, repeatability and parametric analysis. Some models have been developed to investigate the coupled behavior of the CPB, such as the studies of Helinski et al. (2007), Wu et al. (2014), Cui and Fall (2015), and Cui and Fall (2018). Besides, Qi and Fourie (2019) conducted a numerical study to investigate

the effect of the creep behavior of the rock mass on the stress distribution in the backfilled stope. However, these studies did not assess the effect of the CPB coupled behavior on its retaining barricade. Therefore, Cui and Fall (2017) used a more comprehensive model to analyze the barricade pressure evolutions under various backfill cases in the stope. In addition to the investigation of the barricade pressure, this paper will further discuss the deformation of the barricade, in response to the coupled THMC behavior of the CPB. The importance of this study lies in making a contribution to the optimal design of barricade structures and reliable analysis of their stability. Therefore, the core objective of this paper is to develop a numerical model considering the effect of the coupled THMC processes in the CPB, and analyze the evolutions in the barricade pressure and displacement.

2 Governing Equations of the Numerical Model

2.1 Equations for Binder Hydration

Binder hydration is a significant chemical reaction for the consolidation of the CPB, since it can both generate hydration products and hydrating heat to increase the strength and temperature of the CPB. The following equation is used to describe the heat generation process of binder hydration (De Schutter and Taerwe 1996):

$$q_h = q_{\max} \beta_1 \sin(\pi \alpha)^{\beta_2} e^{-\beta_3 \cdot \alpha + \frac{E_a}{R} \cdot \left(\frac{1}{T_r} - \frac{1}{T_c}\right)} \quad (1)$$

where, q_h denotes the specific heat generated by the binder hydration per unit time; q_{\max} represents the maximum value of q_h at 20 °C; β_1 , β_2 , and β_3 are test constants; α is the degree of binder hydration; E_a is the apparent activation energy and its value is dependent on T_c (Jin Sang and Kwang 2001); R is the universal gas constant; T_r is the reference temperature; and T_c is the temperature of the CPB.

The binder hydration degree α can be expressed as follows (Kjellsen and Detwiler 1993; Schindler and Folliard 2005; Poole et al. 2007):

$$\alpha = \alpha_u \cdot \exp \left[- \left(\frac{\tau}{t_e} \right)^\lambda \right] \quad (2)$$

where, τ and λ are fitting parameters, α_u is the ultimate binder hydration degree, and t_e denotes the equivalent age.

The ultimate binder hydration degree α_u can be further written in the following form (Kjellsen et al. 1991):

$$\alpha_u = \frac{1.031 \cdot w/b}{0.194 + w/b} + 0.5p_{FA} + 0.3p_{Slag} \leq 1 \quad (3)$$

where, w/b is the ratio of water-to-binder, and p_{FA} and p_{slag} represent the proportions of fly ash and blast furnace slag in the binder, respectively.

The equivalent age t_e can be expressed as:

$$t_e = \int_0^t \exp \left[\frac{E_a}{R} \cdot \left(\frac{1}{T_r} - \frac{1}{T_c} \right) \right] dt \tag{4}$$

The effect of binder hydration on the strength of the CPB is discussed in the mechanical equations that will be demonstrated in Sect. 2.4.

2.2 Thermal Equations

In addition to the heat of binder hydration, thermal conduction is another significant way that can change the temperature of the CPB, so the following heat transfer equation can be obtained:

$$[(1-\phi)\rho_s C_s + \phi\rho_w C_w] \frac{\partial T}{\partial t} - \nabla \cdot (k_{eq} \nabla T) = m_b q_h \tag{5}$$

where, ϕ is the porosity of the CPB, ρ_s and ρ_w are the solid and water densities, C_s and C_w are the solid and water volumetric heat capacities, k_{eq} is the equivalent thermal conductivity of the CPB, and m_b is the binder content.

The CPB porosity ϕ varies with the evolution of binder hydration degree (Abdul-Hussain and Fall 2011):

$$\phi = \phi_0 + \omega\alpha \tag{6}$$

where, ϕ_0 is the initial porosity of the CPB, and ω is a fitting parameter.

The value of water density is dependent on temperature (Cui and Fall 2015):

$$\rho_w = 314.4 + 685.6 \cdot \left[1 - \left(\frac{T_w - 273.15}{374.14} \right)^{\frac{20}{11}} \right]^{0.55} \tag{7}$$

where, T_w is the water temperature.

2.3 Hydraulic Equations

The following equation can be used to describe the fluid flow in the CPB (Richards 1931; Krus et al. 1997; Taylor et al. 1999; Mainguy et al. 2001; Poyet et al. 2011):

$$\frac{\partial}{\partial t} (\rho_w \phi) + \nabla \cdot \left(\rho_w K \frac{k_r}{\mu_w} p_w \right) = Q_w \tag{8}$$

where, K is the intrinsic permeability of the CPB, μ_w is the dynamic viscosity of water, k_r is the relative permeability of the CPB to water, p_w is the pore water pressure, and Q_w denotes the water drainage.

The intrinsic permeability of the CPB K can be calculated by (Ghirian and Fall 2013):

$$K = K_t \cdot \exp(X\alpha^Y) \tag{9}$$

where, K_t is the hydraulic conductivity of the tailings used, and X and Y are fitting parameters.

The relative permeability of the CPB to water k_r can be expressed by (Mualem 1976; van Genuchten 1980; Luckner et al. 1989):

$$k_r = \sqrt{\frac{\theta_v - \theta_r}{\theta_s - \theta_r}} \cdot \left\{ 1 - \left[1 - \left(\frac{\theta_v - \theta_r}{\theta_s - \theta_r} \right)^{1/m} \right]^m \right\}^2 \tag{10}$$

where, θ_v is the volumetric water content, θ_s and θ_r are respectively the saturated and residual water contents, and m is the material parameter.

The residual water content θ_r can be obtained by (Abdul-Hussain and Fall 2011):

$$\theta_r = \frac{A}{e^{B\alpha}} \tag{11}$$

where, A and B are the fitting constants.

The dynamic viscosity of water μ_w is temperature dependant (Thomas and Sansom 1995):

$$\mu_w = \frac{0.6612}{(T_w - 229)^{1.562}} \tag{11}$$

2.4 Mechanical Equations

The total pressure (p_t) at any point of the CPB in the depth of H can be expressed as follows:

$$p_t = \rho_c g H \tag{12}$$

where, ρ_c is the CPB density.

The effective pressure (p_{eff}) in the CPB can be written as follows:

$$p_{eff} = p_t - \phi p_w \delta_{ij} \tag{13}$$

where, δ_{ij} is the Kroenecker's delta: $\delta_{ii}=1$; $\delta_{i \neq j}=0$.

The horizontal pressure (p_h) can be calculated by:

$$p_h = \frac{\nu}{1-\nu} (\rho_c g H - \phi p_w \delta_{ij}) \tag{14}$$

where, ν is the Poisson's ratio, which can be further expressed in the following form (Sayers and Grenfell 1993; Boumiz et al. 1996; Bittnar 2006; Galaa et al. 2011):

$$\nu = 0.5 \cdot \exp(f_1 \alpha) + f_2 \alpha^{f_3} \cdot \exp(f_4 \alpha^{f_5}) \tag{15}$$

The following equation is applied to calculate the displacement induced by the hydro-mechanical coupling effect (Zhang et al. 2012):

$$\frac{E}{2(1+\nu)} \nabla^2 u + \frac{E}{2(1+\nu)(1-2\nu)} \nabla \cdot (\nabla u) = \alpha_b \rho_w g \nabla p_t \tag{16}$$

where, E is the elastic modulus, u is the displacement vector, and α_b is the Biot's effective stress coefficient (Cui and Fall 2017):

$$\alpha_b = 1 - \frac{E}{3K_t(1-2\nu)} \tag{17}$$

where, K_t is the bulk modulus of the tailings.

The elastic modulus E varies with the progress of binder hydration (De Schutter and Taerwe 1996):

$$E = E_u \left(\frac{\alpha - \alpha_0}{\alpha_u - \alpha_0} \right)^n \tag{18}$$

where, E_u is the elastic modulus when α is equal to 1; α_0 is a certain value of the binder hydration degree, below which no strength develops in the CPB; n is a fitting constant.

The equations for binder hydration, thermal, hydraulic and mechanical equations can be integrated together to form a coupled numerical model, via the linkage of the evolution of the binder hydration degree with time. Since the degree of binder hydration also varies with temperature, the coupled model is dynamically dependent on temperature and time.

3 Validation of the Developed Model

In order to validate the capability of the developed model in predicting the barricade mechanical performance, two sets of field monitoring data acquired from two different mines were selected to compare with the model simulation results. Table 1 lists the input parameters, boundary conditions and initial values used for the model validation.

3.1 Field Case 1

3.1.1 Overview of the Stope Conditions

Thompson et al. (2010) conducted a field monitoring study at Cayeli Bakir Isletmeleri A.S. (CBI) mine, which was an underground mine producing copper and zinc. The total applied pressure and displacement data of the barricade at Stope 685N20 of this mine were used for the model validation. Table 2 summarizes some information of the backfill conditions.

The construction information of the barricade can be found in the referred study (Thompson et al. 2010). Figure 1 shows a three-dimensional (3D) mesh model of the barricade at Stope 685N20, and Fig. 2 demonstrates a 3D schematic diagram for the filling of Stope 685N20.

In order to monitor the stress and displacement changes of the barricade, three total earth pressure cells

Table 1 Input parameters, boundary conditions and initial values used for validating the developed model.

	Field case 1	Field case 2
Initial CPB temperature	29 °C	25 °C
Environment temperature	29 °C	25 °C
Density of CPB	2050 kg/m ³	1900 kg/m ³
Density of concrete	2500 kg/m ³	2263 kg/m ³
Young's modulus of concrete	30 GPa	30 GPa
Poisson's ratio of concrete	0.2	0.2
q_{max}	2.19 W/kg	2.19 W/kg
β_1	2.6	2.6
β_2	0.667	0.667
β_3	3.0	3.0
α_0	0	0
τ	0.6 h	0.6 h
λ	30	30
X	-8.173	-8.173
Y	4.035	4.035
A	1.31	1.31
B	7.54	7.54
f_1-f_5	-0.2, -15,000, 7, -11, 0.7	-0.2, -15,000, 7, -11, 0.7
n	2.2	2.2
Mechanical module for the barricade		
Top surface	Fixed	Fixed
Lateral sides (contact with rock)	Roller	Roller
Lateral sides (contact with CPB)	Free	Free
Lateral sides (contact with air)	Free	Free
Bottom side	Fixed	Fixed
Volume force	Gravity	Gravity

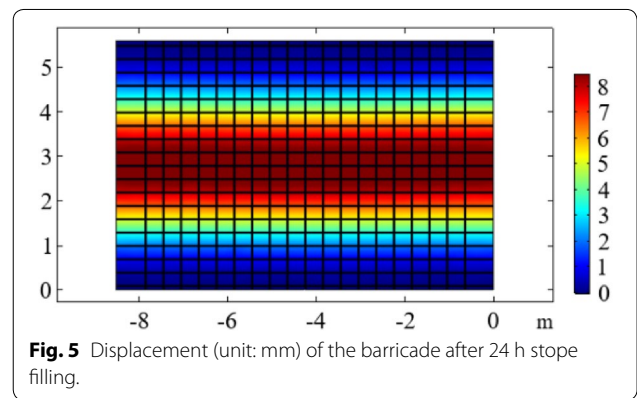
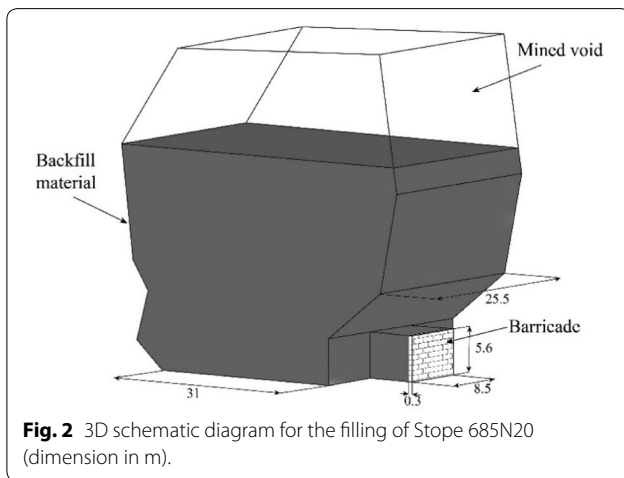
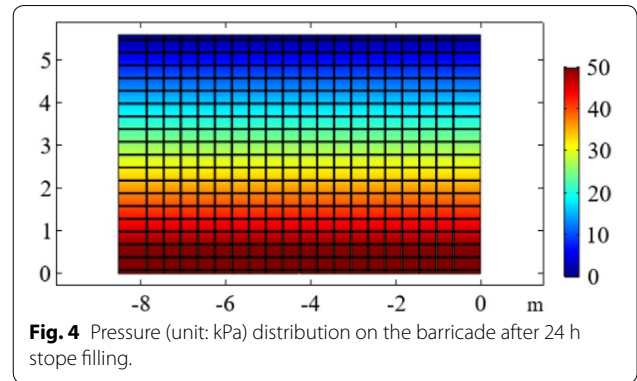
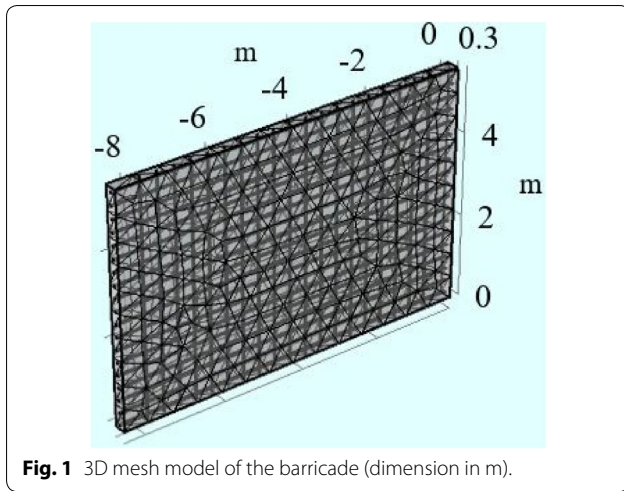
The reference studies (De Schutter and Taerwe 1996; Thompson et al. 2009, 2010; Abdul-Hussain and Fall 2011; Ghirian and Fall 2013; Cui and Fall 2016).

Table 2 Information of the backfill conditions for field case studies.

	Field case 1	Field case 2
Binder content (%)	8.5 (0–8 m) 6.5 (8–15 m)	4 (0–6 m) 2 (6–32 m)
Filling rate (cm/h)	23	50
Filling strategy	Continuous fill	Continuous fill
Barricade size (m)	5.6 (height) 0.3 (thickness) 8.5 (extent)	5.8 (height) 0.3 (thickness)

The reference studies (Thompson et al. 2009, 2010).

(TEPCs) and six displacement sensors were installed on the barricade for measuring the total applied horizontal pressure and displacement of the barricade, as shown in Fig. 3. The transducers D1, D3 and D5 sensors were



placed at the height of 1.4 m, and D2, D4 and D6 were at 2.8 m, and the horizontal distance between the displacement sensors was 1.25 m.

3.1.2 Model Simulation and Validation

Firstly, the 3D geometric model of the stope (including the barricade) is imported into COMSOL (2015), and then the barricade is divided with separate domain. Secondly, the relevant equations, parameters and initial values (as shown in Tables 1 and 2) are input, and the boundary conditions are installed. Thirdly, the meshing for the geometric model is completed. Finally, the transient calculation is conducted. During the post-processing program, the distribution of pressure and displacement on the barricade, and their evolutions at the given points corresponding to the positions of field sensors are investigated.

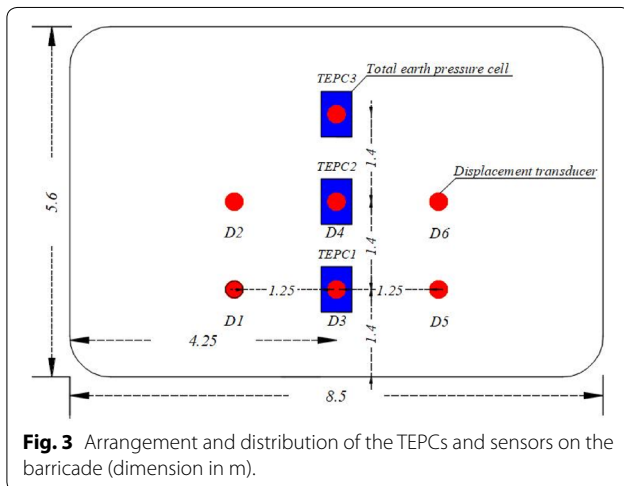
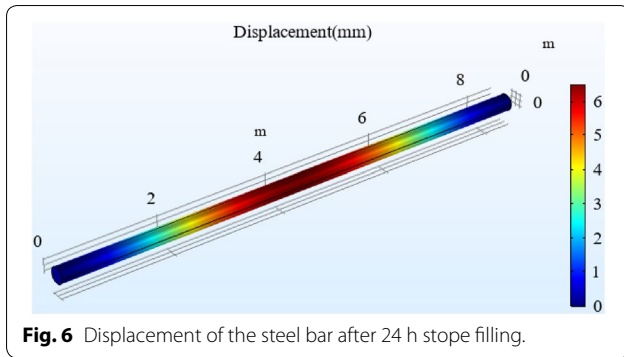


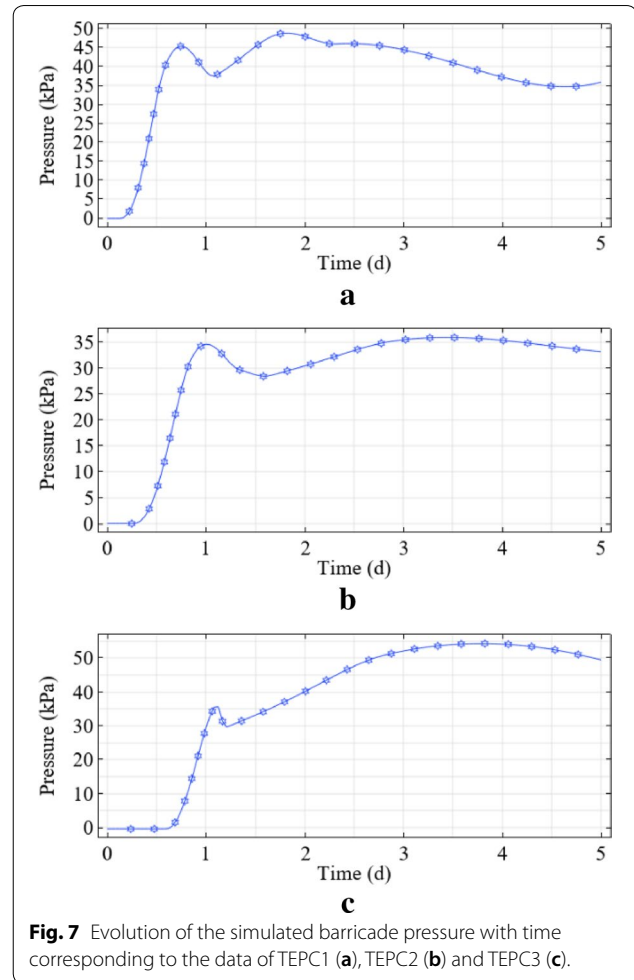
Figure 4 shows the pressure distribution on the barricade in the early age (24 h), and Fig. 5 displays the displacement of the barricade after 24 h stope filling. It can be observed from Fig. 4 that the pressure distribution on the barricade follows the trend of increasing gradually from the top to the bottom, and Fig. 5 indicates that the maximum displacement of the barricade appears at the center of the barricade. It can be inferred



that during the filling process, the pressure on the barricade is mainly affected by the filling of the CPB, which can be understood as that the CPB applies pore water pressure onto the barricade in the form of fluid, and pore water pressure is an integral part of the effective stress, so as to cause this distribution of the pressure. In addition, steel bars are embedded in the surrounding rock before casting concrete to construct the barricade. Therefore, the barricade is fixed along its four edges, and the maximum displacement is mainly distributed at the center of the barricade.

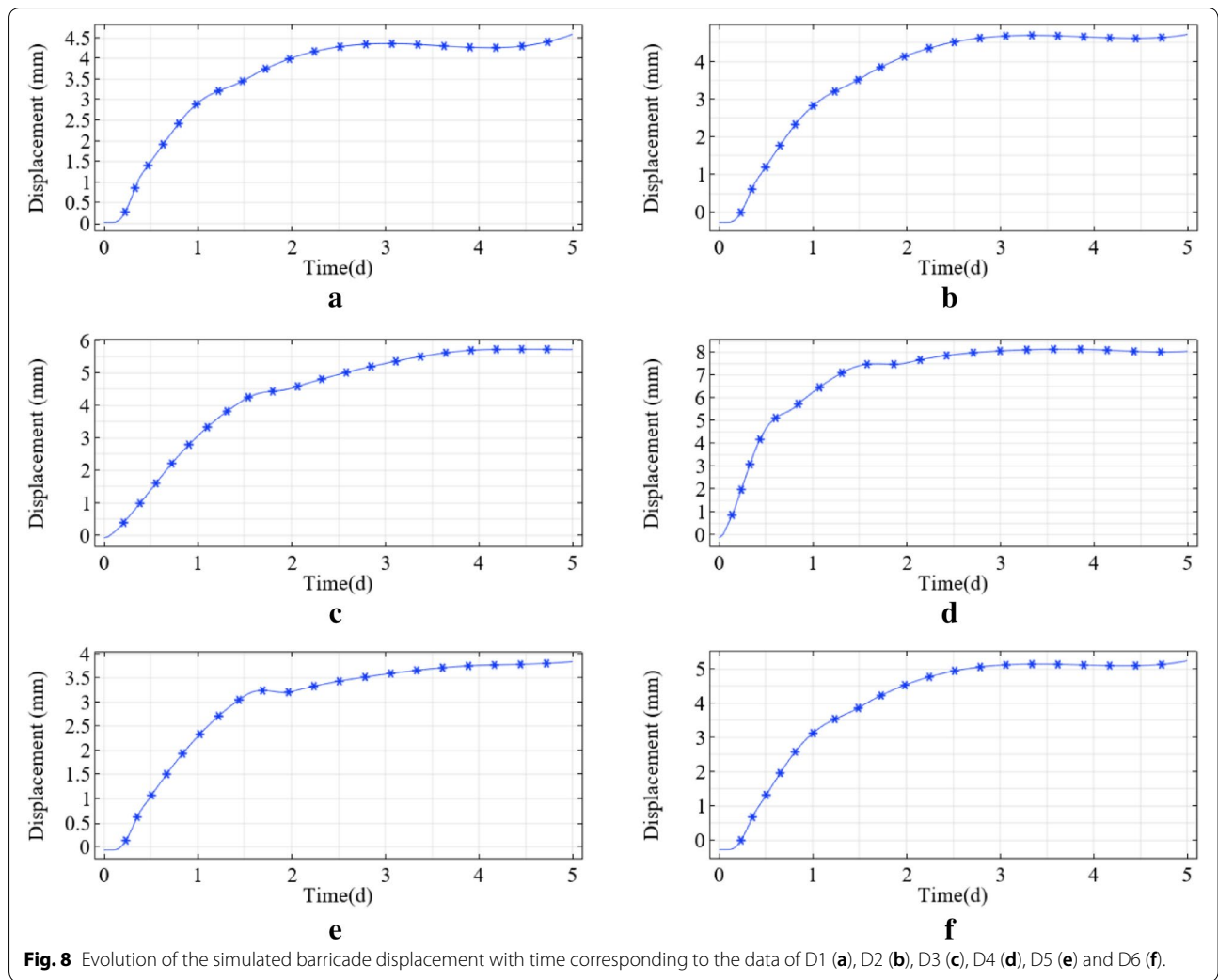
Figure 6 shows the deformation of the horizontal steel bar at the center of the barricade under pressure. It can be observed from this figure that when the barricade is subjected to the pressure, the steel bar has the maximum displacement in the middle part. This can demonstrate the phenomenon of stress concentration at the center of the barricade.

For further analyzing the evolutions of the barricade pressure and displacement, the monitoring points corresponding to the field measurement are arranged on the barricade geometric model, and the transient change data of the barricade pressure and displacement are recorded and displayed. Figure 7 illustrates the simulation results of the barricade pressure evolution versus time. It can be noticed from this figure that in the initial stage of the stope filling, the barricade pressure follows a continuous rise until it reaches the first peak value. The predicted barricade pressure corresponding to the data of TEPC1 reaches the first peak value of 45.5 kPa in about 0.8 d, while that of TEPC2 reaches 34.6 kPa in about 1.0 d, and that of TEPC3 reaches 35.3 kPa in about 1.1 d. The rise of the barricade pressure in this stage can be attributed to the continuous pouring of the CPB slurry. The CPB slurry mainly poses pore water pressure on the barricade and causes an obvious increase in the pressure of TEPC1. After a short period of time, the barricade pressure slightly decreases. This is because of the barricade



water drainage. The pressure growth indicated by TEPC3 is the most obvious. After reaching the second peak of 54.5 kPa, the total stress gradually decreases to the value of 49.8 kPa, while the pressures of TEPC1 and TEPC2 reduce from 48.6 kPa and 36.1 kPa to 35.2 kPa and 32.8 kPa, respectively. The reason is attributed to the fact that with the consolidation process of CPB, arching of pressure within the CPB occurs, reducing the effect of the CPB self weight on the barricade pressure. In addition, the influence of pore water pressure on the total stress further reduces with the progress of the barricade water drainage and the water consumption induced by the binder hydration. These facts result in the decrease of the barricade pressure in the later period of the monitoring course.

Figure 8 demonstrates the barricade displacement evolution versus time predicted by the developed model, corresponding to the data collected from the displacement sensors in the filed measurement. From Fig. 8 it can be seen that the barricade displacement increases with time. Figures 7 and 8 indicate that there



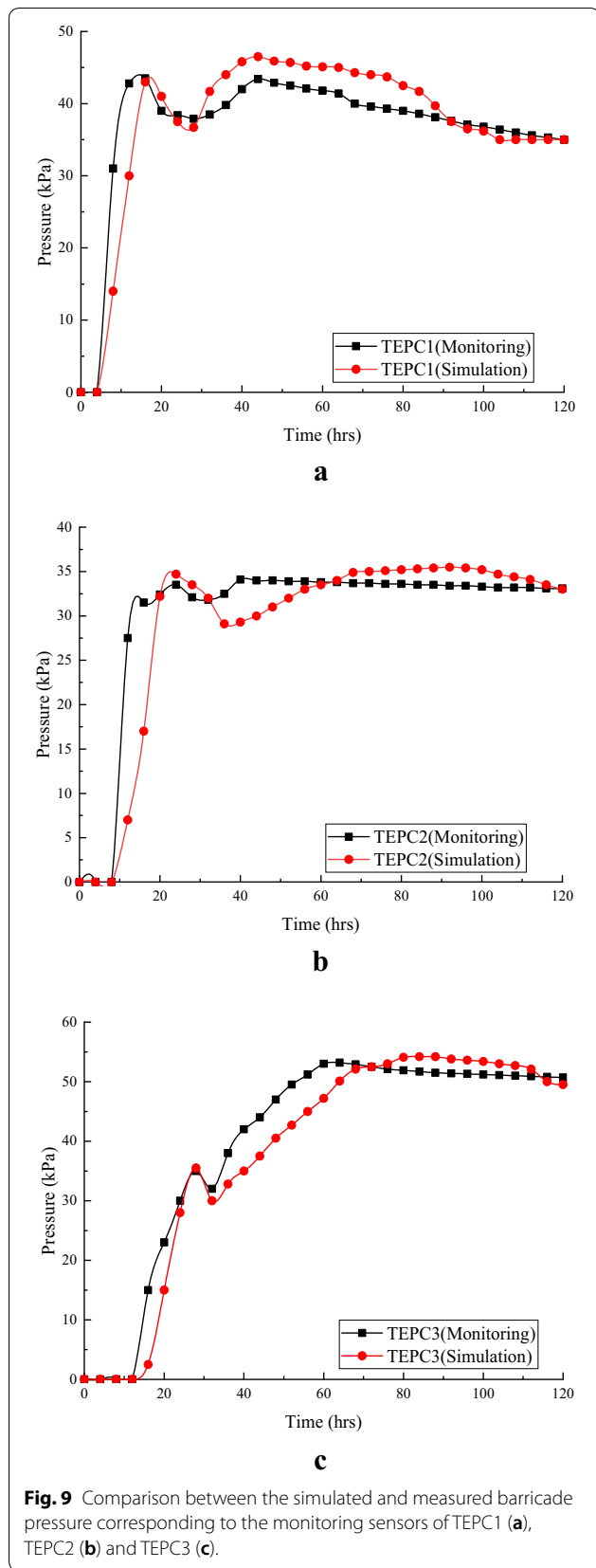
is a positive correlation between the evolutions of the barricade pressure and displacement versus time.

The barricade pressure and displacement predicted by the model simulation are compared with the field monitoring data, for verifying the validity of the developed model. The comparison between the simulation results and measured data of the barricade pressure is demonstrated in Fig. 9. It can be seen from this figure that the developed model can accurately capture the evolution of the total stress on the barricade, and the change range and trend of the simulation results coincide with the measured data in favorable consistency. It can also be observed that regardless of the predicting or monitoring outcomes, with the filling of the CPB, the barricade pressure increases sharply in the early age. After a slight decrease in the barricade pressure, it rises again until a constant value is maintained. The comparison results prove the capability of the developed model in

predicting the barricade pressure evolution, which also reflects the state of the CPB and its THMC behavior.

Figure 10 illustrates the comparison between the simulated and measured barricade displacement. The model simulation results of the barricade displacement and the correspondingly monitored data are in satisfactory consistency, except for some misfits that are in an acceptable range. The contrast results further verify the validity of the developed model in simulating the mechanical response of the barricade to the coupled processes that occur in the placed CPB.

Figure 11 shows the comparison of the maximum barricade displacement between the predicted and measured outcomes. It is noticed from this figure that due to the fixed four edges of the barricade, the maximum displacements at D2, D4 and D6 are greater than that at D1, D3 and D5. It can also be seen that the model prediction results agree well with the field



monitoring data, verifying the effectiveness of the simulation results.

3.2 Field Case 2

Thompson et al. (2009) carried out another field monitoring program at 67-SL1 test stope of Kidd Mine. The pressure data collected by the sensors of C1-C4 (as shown in Fig. 12) and the barricade displacement data of B1-B3 (Fig. 12) were selected for comparing with the predicted results. Some information about the 67-SL1 stope fill conditions can be found in Table 2. Detailed information of the barricade and binder used can be identified in the referred study (Thompson et al. 2009).

The stress distribution in the test stope after different filling time is shown in Fig. 13. In the early filling age (3 days), due to the settlement of the CPB, the stress is mainly distributed at the bottom of the stope. In the late filling period (6 d), the stress is uniformly distributed within the stope. The stress distribution near the barricade is scattered, which may be caused by the pressure arching effect.

For further validating the availability of the developed model, the simulation results are compared with the correspondingly measured data from Kidd Mine, in terms of the pressure development as shown in Fig. 14 and displacement evolution in Fig. 15.

From Fig. 14 it can be observed that the predicted pressure development in the stope agrees well with the measured data, in terms of the evolutionary trend and peak value. The misfits between the simulation and measurement are acceptable, with all the deviations less than 5%. The favorable consistency indicates the availability of the developed model in predicting the stress development in the CPB.

Figure 15 illustrates the comparison of the barricade displacement evolutions between the simulation and in situ measurement. It is seen from this figure that the simulation results and measured data are basically in agreement, except for some incongruence in terms of the results from B3, which may be due to the varied boundary conditions in the field. The comparison outcomes prove the validity of the developed model in simulating the barricade displacement.

4 Model Application

The model validation results indicate that the developed model can well predict the pressure and displacement of the backfill barricade in response to the coupled THMC behavior of the CPB. In this section, the developed model is employed to analyze an important engineering problem in practice: effect of filling strategy on the barricade performance.

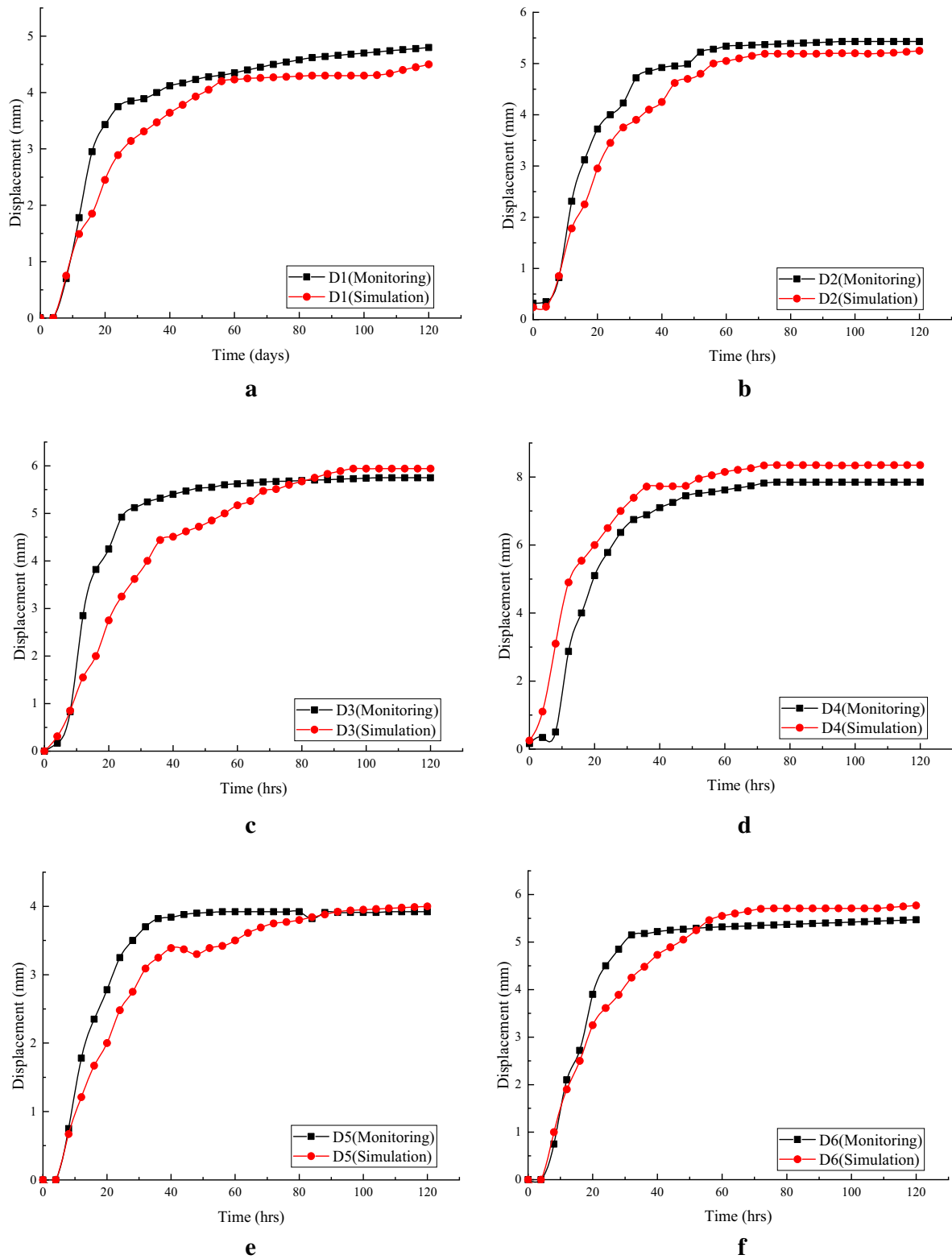
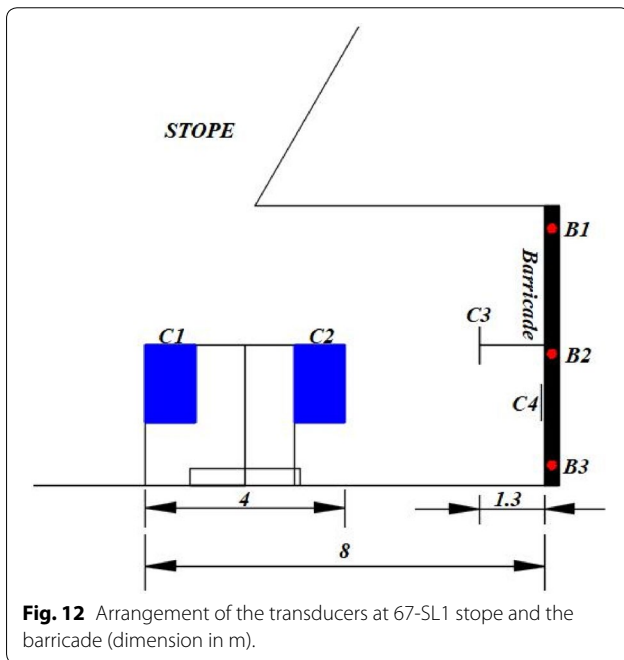
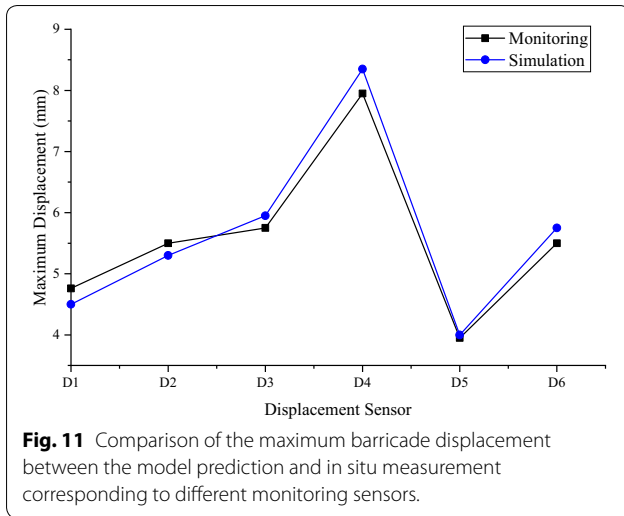


Fig. 10 Comparison between the predicted and measured barricade displacement corresponding to the monitoring transducers of D1 (a), D2 (b), D3 (c), D4 (d), D5 (e) and D6 (f).



A parametric study based on the 685N20 stope is carried out to reveal the impact of various backfill conditions on the barricade mechanical behavior. Since the barricade pressure and displacement have a positive correlation, the displacement of the barricade can accurately reflect the barricade pressure. Therefore, the maximum displacement of the barricade is investigated in the following parametric research.

The continuous filling (at the filling rate of 17 cm/h, 23 cm/h and 35 cm/h) and discontinuous filling (at the filling rate of 29 cm/h during 0–24 h, 29–48 h and 53–120 h, and the rest period is 24–29 h and 48–53 h)

strategies are selected to conduct this simulation. The maximum barricade displacement collected at the monitoring point of D4 (as shown in Fig. 3) with different filling conditions is investigated, as illustrated in Fig. 16. It can be clearly observed that the maximum barricade displacement increases with the filling rate of the CPB, and the discontinuous filling method can slow down the development of the barricade displacement during the rest period.

The results revealed by Fig. 16 indicate that, the change of the filling rate can significantly affect the barricade displacement. It can be noticed that the filling method also affects the barricade displacement, and the rest period can slow down the increase of the barricade displacement at a relatively high filling rate. The model simulation results contribute to important practical implication: when a high filling rate is applied, a rest period can be properly arranged to reduce the increase in the barricade displacement; while if the backfilling is at a low rate, the resting period can be decreased or even canceled. A reasonable arrangement of the filling rate and filling strategy can provide well economic benefits in accordance with the barricade stability.

5 Conclusions

In this paper, a numerical model is developed to characterize and describe the mechanical response of the barricade to the coupled THMC behavior of in situ CPB. The developed model considers the binder hydration process, thermal process of heat generation and conduction, hydraulic process of pore water pressure evolution and water drainage, and mechanical process of stress and displacement development. The monitoring data from two field case studies are employed to compare with the corresponding results predicted by the model simulation. On the basis of the obtained results, the following conclusions can be drawn:

- i. Satisfactory agreements are found between the model prediction results and in situ monitoring data, verifying the validity and capability of the developed model in analyzing the barricade stress and displacement.
- ii. The barricade pressure is significantly affected by the coupled THMC processes that occur in the CPB, and it also varies with the consolidation process of the CPB. In the early stage of backfilling, the placed CPB applies pressure on the barricade in the form of fluid, and the barricade pressure is relative to the temperature, pore water pressure, weight of CPB and binder hydration. However, when the placed CPB is hardened and self-supporting, no pressure is applied on the barricade.

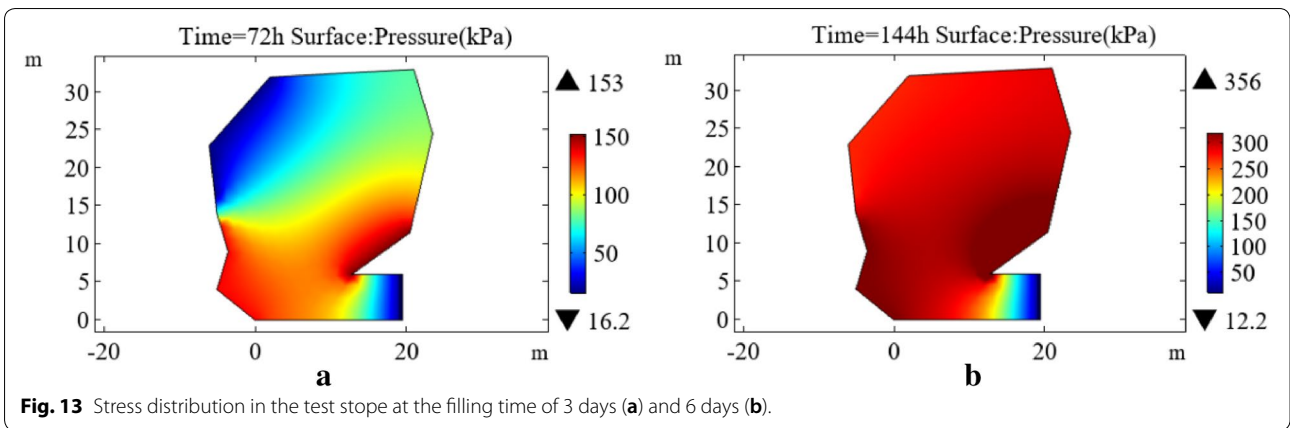


Fig. 13 Stress distribution in the test stope at the filling time of 3 days (a) and 6 days (b).

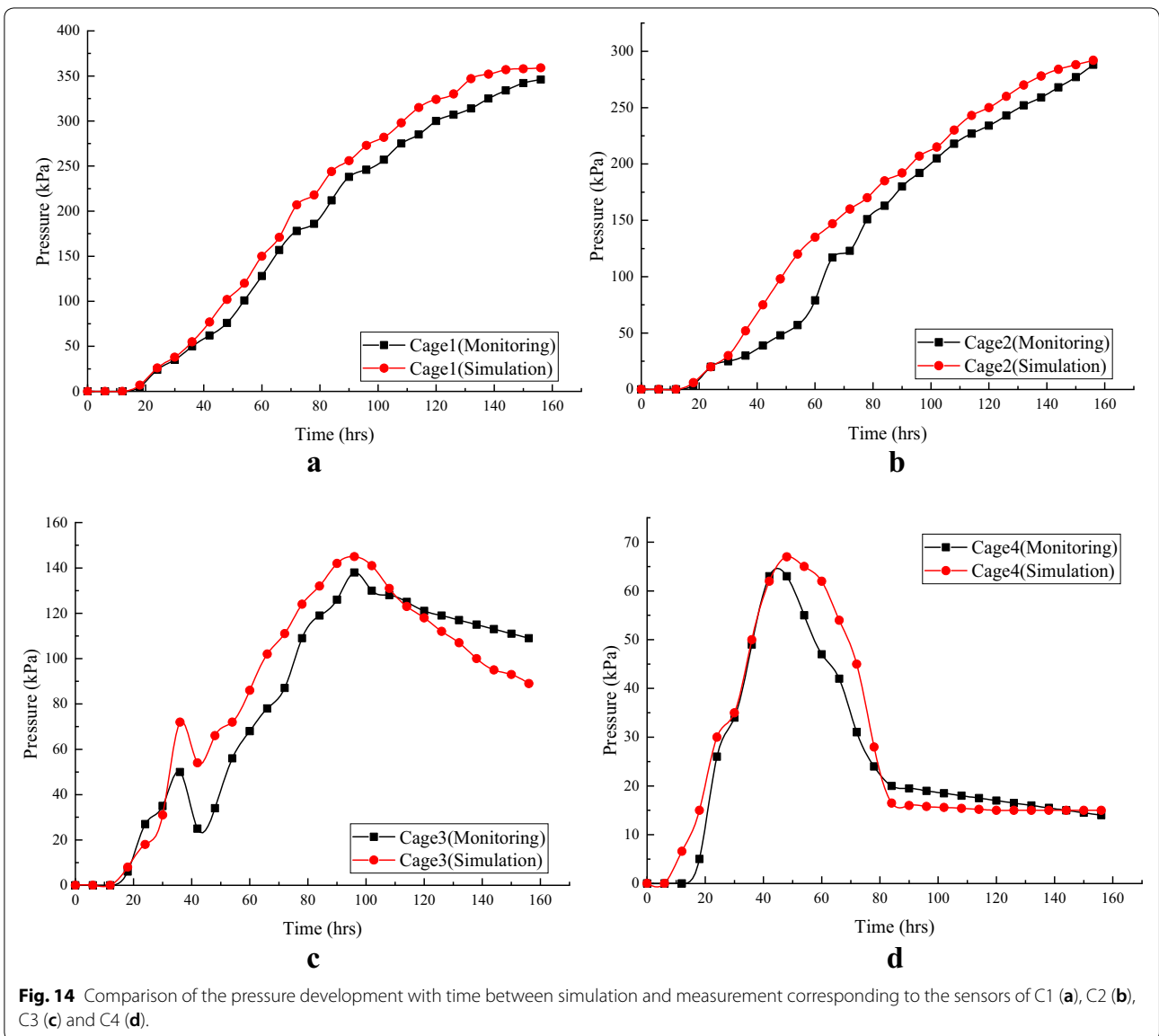
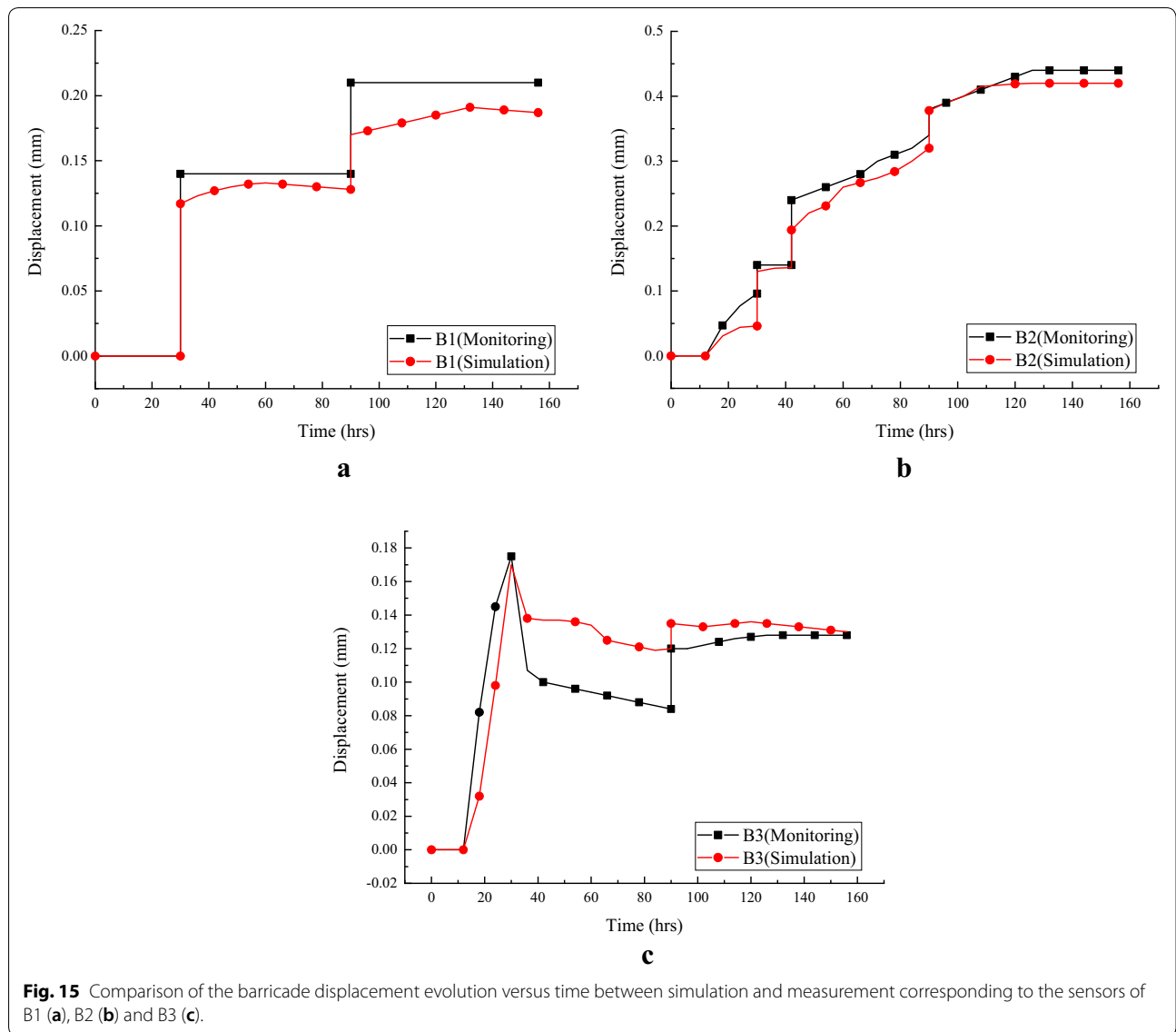
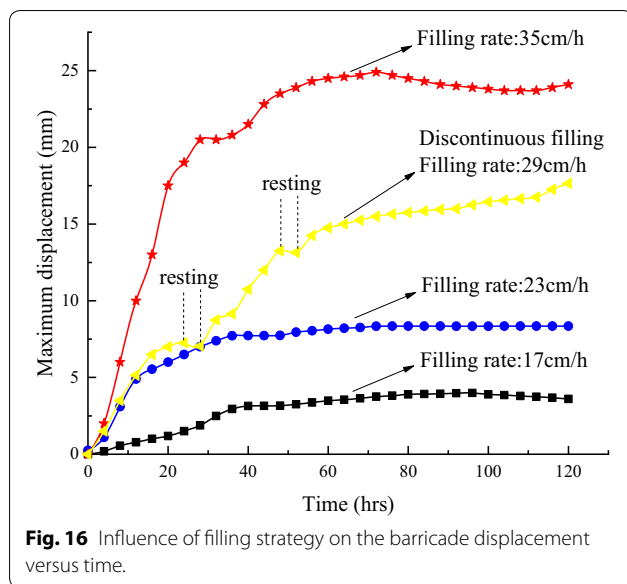


Fig. 14 Comparison of the pressure development with time between simulation and measurement corresponding to the sensors of C1 (a), C2 (b), C3 (c) and C4 (d).



- iii. There is a positive correlation between the displacement and pressure of the barrage. In the early stage of the rapid pressure rise induced by the pouring of the fresh CPB, the barrage displacement also increases obviously. The barrage displacement stabilizes as the pressure tends to be stable.
- iv. Conspicuous displacement is found distributing in the central area of the barrage. Hence, the center of the barrage can be reinforced accordingly to improve the barrage stability.
- v. The barrage pressure and displacement are observably affected by the filling rate and backfill strategy, so the filling rate and rest period can be scheduled to maintain the barrage stability.

Although this paper develops a numerical model to analyze the mechanical response of the barrage to the coupled behavior of the CPB in the stope, the application of the model is limited. For instance, the effect of stope size and geometry on the barrage performance is not discussed. Therefore, a future study is going to investigate the barrage behavior, in consideration of the interaction between the CPB and stope. In addition, the model simulation work is expected to be extended to the design of stable and cost-effective barrage structure.



Acknowledgements

The authors would like to acknowledge the support from China Scholarship Council; Yue Qi Young Scholar Project, China University of Mining and Technology, Beijing; and The University of Western Australia.

Authors' contributions

DW made a contribution to conception, design of the work and revised the manuscript. WH made a contribution to develop the numerical model and drafted the manuscript. SL made a contribution to the model simulation and validation. HL made a contribution to the model application. All authors read and approved the final manuscript.

Author's information

Di Wu, Associate Professor at: School of Energy and Mining Engineering, China University of Mining and Technology-Beijing, China. His research interests include mine backfill, coupled modeling in geotechnical engineering, and mine waste management. Wentao Hou, Master's Student of Mining Engineering at: School of Energy and Mining Engineering, China University of Mining and Technology-Beijing, China. He is supervised by Di Wu. Shuai Liu, Master's Student of Mining Engineering at: School of Energy and Mining Engineering, China University of Mining and Technology-Beijing, China. He is supervised by Di Wu. Huaibin Liu, Master's Student of Mining Engineering at: School of Energy and Mining Engineering, China University of Mining and Technology-Beijing, China. He is supervised by Di Wu.

Funding

This investigation was supported by the following funders, and their role of the funding body was declared as follow:

1. China Scholarship Council (No. 201806435003): the support for the visit of The University of Western Australia and thus the initiation of the study;
2. Yue Qi Young Scholar Project, China University of Mining and Technology, Beijing: writing the manuscript.

Availability of data and materials

All data generated or analyzed during this study are included in this published article.

Ethics approval and consent to participate

The corresponding author would like to declare on behalf of the co-authors that the work described is original research that has not been published previously, and not under consideration for publication elsewhere, in whole or in part.

Competing interests

No competing interests exists in the submission of this manuscript, and manuscript is approved by all authors for publication. The author declare that the work described was original research that has not been published previously, and not under consideration for publication elsewhere, in whole or in part.

Received: 20 January 2020 Accepted: 26 April 2020

Published online: 14 August 2020

References

- Abdul-Hussain, N., & Fall, M. (2011). Unsaturated hydraulic properties of cemented tailings backfill that contains sodium silicate. *Engineering Geology*, 123(4), 288–301.
- Belem, T., Harvey, A., Simon, R., Aubertin, M. (2004). Measurement of internal pressures of a gold mine pastefill during and after the stope backfilling. In: 5th International symposium on ground support in mining and underground construction, pp. 619–630.
- Bittnar, Z. (2006). Microstructure-based micromechanical prediction of elastic properties in hydrating cement paste. *Cement and Concrete Research*, 36(9), 1708–1718.
- Boumiz, A., Vernet, C., & Tenoudji, F. C. (1996). Mechanical properties of cement pastes and mortars at early ages: Evolution with time and degree of hydration. *Advanced Cement Based Materials*, 3(3), 94–106.
- COMSOL. (2015). COMSOL Multiphysics 5.1, <http://www.comsol.com>.
- Cui, L., & Fall, M. (2015). A coupled thermo-hydro-mechanical-chemical model for underground cemented tailings backfill. *Tunnelling and Underground Space Technology*, 50, 396–414.
- Cui, L., & Fall, M. (2016). An evolutive elasto-plastic model for cemented paste backfill. *Computers and Geotechnics*, 71, 19–29.
- Cui, L., & Fall, M. (2017). Modeling of pressure on retaining structures for underground fill mass. *Tunnelling and Underground Space Technology*, 69, 94–107.
- Cui, L., & Fall, M. (2018). Multiphysics modeling and simulation of strength development and distribution in cemented tailings backfill structures. *International Journal of Concrete Structures and Materials*, 12, 25. <https://doi.org/10.1186/s40069-018-0250-y>.
- De Schutter, G., & Taerwe, L. (1996). Degree of hydration-based description of mechanical properties of early age concrete. *Materials and Structures*, 29(6), 335–344.
- Doherty, J. P. (2015). A numerical study into factors affecting stress and pore pressure in free draining mine stopes. *Computers and Geotechnics*, 63, 331–341.
- Doherty, J. P., Hasan, A., Suazo, G. H., & Fourie, A. (2015). Investigation of some controllable factors that impact the stress state in cemented paste backfill. *Canadian Geotechnical Journal*, 52, 1901–1912.
- Ercikdi, B., Kesimal, A., Cihangir, F., Deveci, H., & Alp, I. (2009). Cemented paste backfill of sulphide-rich tailings: Importance of binder type and dosage. *Cement and Concrete Composites*, 31, 268–274.
- Fall, M., Benzaazoua, M., & Ouellet, S. (2005). Experimental characterization of the effect of tailings fineness and density on the quality of cemented paste backfill. *Minerals Engineering*, 18, 41–44.
- Fall, M., Benzaazoua, M., & Sae, E. (2008). Mix proportioning of underground cemented paste backfill. *Tunnelling and Underground Space Technology*, 23, 80–90.
- Fall, M., & Pokharel, M. (2010). Coupled effects of sulphate and temperature on the strength of CPB. *Cement and Concrete Composites*, 32(10), 819–928.
- Galaa, A. M., Thompson, B. D., Grabinsky, M. W., & Bawden, W. F. (2011). Characterizing stiffness development in hydrating mine backfill using ultrasonic wave measurements. *Canadian Geotechnical Journal*, 48(8), 1174–1187.
- Ghirian, A., & Fall, M. (2013). Coupled thermo-hydro-mechanical-chemical behavior of cemented paste backfill in column experiments. Part I: Physical, hydraulic and thermal processes and characteristics. *Engineering Geology*, 164, 195–207.
- Helinski, M., Fahey, M., & Fourie, A. (2007). Numerical modeling of cemented mine backfill deposition. *Journal of Geotechnical and Geoenvironment*, 133, 1308–1319.

- Helinski, M., Fahey, M., & Fourie, A. (2011). Behavior of cemented paste backfill in two mine stopes: Measurements and modeling. *Journal of Geotechnical and Geoenvironmental Engineering*, 137, 171–182.
- Jin Sang, H. H., & Kwang, M. L. (2001). Estimation of compressive strength by a new apparent activation energy function. *Cement and Concrete Research*, 31(2), 217–225.
- Kesimal, A., Arcikdi, B., & Yilmaz, E. (2003). The effect of desliming by sedimentation on paste backfill performance. *Minerals Engineering*, 16, 1009–1011.
- Kjellsen, K. O., & Detwiler, R. J. (1993). Later-age strength prediction by a modified maturity model. *ACI Materials Journal*, 90(3), 220–227.
- Kjellsen, K. O., Detwiler, R. J., & Gjrv, O. E. (1991). Development of microstructures in plain cement pastes hydrated at different temperatures. *Cement and Concrete Research*, 21(1), 179–189.
- Krus, M., Hansen, K. K., & Kiinzel, H. M. (1997). Porosity and liquid absorption of cement paste. *Materials and Structures*, 30, 394–398.
- Luckner, L., van Genuchten, M. T., & Nielsen, D. R. (1989). A consistent set of parametric models for the two-phase flow of immiscible fluids in the subsurface. *Water Resources Research*, 25(10), 2187–2193.
- Mahlaba, J. S., Kearsley, E. P., Richard, A., & Kruger, R. A. (2011). Physical, chemical and mineralogical characterisation of hydraulically disposed fine coal ash from SASOL Synfuels. *Fuel*, 90(7), 2491–2500.
- Mainguy, M., Coussy, O., & Baroghel-Bouny, V. (2001). Role of air pressure in drying of weakly permeable materials. *Journal of Engineering Mechanics*, 127, 582–592.
- Mualem, Y. (1976). A new model for predicting the hydraulic conductivity of unsaturated porous media. *Water Resources Research*, 12, 513–522.
- Pokharel, M., & Fall, M. (2013). Combined influence of sulphate and temperature on the saturated hydraulic conductivity of hardened cemented paste backfill. *Cement and Concrete Composites*, 38, 21–28.
- Poole, J. L., Riding, K. A., Folliard, K. J., Juenger, M. C. G., & Schindler, A. K. (2007). Methods for calculating activation energy for Portland cement. *ACI Materials Journal*, 104(1), 303–311.
- Poyet, S., Charlesa, S., Honor, N., & L'hostisa, V. (2011). Assessment of the unsaturated water transport properties of an old concrete: Determination of the pore-interaction factor. *Cement and Concrete Research*, 41, 1015–1023.
- Qi, C., & Fourie, A. (2019). Numerical investigation of the stress distribution in backfilled stopes considering creep behaviour of rock mass. *Rock Mechanics and Rock Engineering*, 52, 3353–3371.
- Richards, L. A. (1931). Capillary conduction of liquids through porous mediums. *Physics*, 1, 318–333.
- Sayers, C., & Grenfell, R. (1993). Ultrasonic propagation through hydrating cements. *Ultrasonics*, 31(3), 147–153.
- Schindler, A. K., & Folliard, K. J. (2005). Heat of hydration models for cementitious materials. *ACI Materials Journal*, 102(1), 24–33.
- Taylor, S. C., Hoff, W. D., Wilson, M. A., & Green, K. M. (1999). Anomalous water transport properties of Portland and blended cement-based materials. *Journal of Material Science Letters*, 18, 1925–1927.
- Thomas, H. R., & Sansom, M. R. (1995). Fully coupled analysis of heat, moisture, and air transfer in unsaturated soil. *Journal of Engineering Mechanics*, 121, 392–405.
- Thompson, B. D. (2010). *Fieldwork report for paste backfill project at Cayeli Bakir Mine*. Turkey: University of Toronto.
- Thompson, B. D., Bawden, W. F., & Grabinsky, M. W. (2012). In situ measurements of cemented paste backfill at the Cayeli Mine. *Canadian Geotechnical Journal*, 49, 755–772.
- Thompson, B.D., Grabinsky, M.W., Bawden, W.F., Counter, D.B., 2009. In-situ measurements of cemented paste backfill in long-hole stopes. In Proceedings of the 3rd CANUS Rock Mechanics Symposium, Toronto, Ont. Paper 4061.
- van Genuchten, M. T. (1980). A closed-form equation for predicting the hydraulic conductivity of unsaturated soils. *Soil Science Society of America Journal*, 44(5), 892–898.
- Wu, D., Fall, M., & Cai, S. (2014). Numerical modelling of thermally and hydraulically coupled processes in hydrating cemented tailings backfill columns. *International Journal of Mining, Reclamation and Environment*, 28, 173–199.
- Yumlu, M., Guresci, M., 2007. Paste backfill bulkhead monitoring—a case study from Inmet's Cayeli mine, Turkey. In Proceedings of the 9th international symposium on mining with backfill, Montral. Paper 28.
- Zhang, B., Li, W., Feng, F., Wu, B., & Cao, X. (2012). Numerical simulation for fluid-solid coupling characteristics in surrounding rock of underground water-sealed oil storage based. *Journal of Engineering Geology*, 5, 789–795.

Publisher's Note

Springer Nature remains neutral with regard to jurisdictional claims in published maps and institutional affiliations.

Submit your manuscript to a SpringerOpen[®] journal and benefit from:

- Convenient online submission
- Rigorous peer review
- Open access: articles freely available online
- High visibility within the field
- Retaining the copyright to your article

Submit your next manuscript at ► [springeropen.com](https://www.springeropen.com)
